Journal of Power Sources 196 (2011) 1295–1302

Contents lists available at ScienceDirect

Journal of Power Sources

journal homepage: www.elsevier.com/locate/jpowsour

Power decoupling control of a solid oxide fuel cell and micro gas turbine hybrid power system

Xiao-Juan Wu[a,*], Qi Huang[a], Xin-Jian Zhu[b]

[a] School of Automation, University of Electronic Science and Technology of China, Chengdu 610054, China
[b] Institute of Fuel Cell, Shanghai Jiao Tong University, Shanghai 200030, China

ARTICLE INFO

Article history:
Received 26 July 2010
Accepted 29 July 2010
Available online 7 August 2010

Keywords:
Solid Oxide Fuel Fell (SOFC)
Micro Gas Turbine (MGT)
Output–input feedback (OIF)
Elman neural network
Particle swarm optimization (PSO)
Proportional-integral-derivative (PID)
decoupling control

ABSTRACT

Solid Oxide Fuel Cell (SOFC) integrated into Micro Gas Turbine (MGT) is a multivariable nonlinear and strong coupling system. To enable the SOFC and MGT hybrid power system to follow the load profile accurately, this paper proposes a self-tuning PID decoupling controller based on a modified output–input feedback (OIF) Elman neural network model to track the MGT output power and SOFC output power. During the modeling, in order to avoid getting into a local minimum, an improved particle swarm optimization (PSO) algorithm is employed to optimize the weights of the OIF Elman neural network. Using the modified OIF Elman neural network identifier, the SOFC/MGT hybrid system is identified on-line, and the parameters of the PID controller are tuned automatically. Furthermore, the corresponding decoupling control law is achieved by the conventional PID control algorithm. The validity and accuracy of the decoupling controller are tested by simulations in MATLAB environment. The simulation results verify that the proposed control strategy can achieve favorable control performance with regard to various load disturbances.

1. Introduction

With increasing global energy needs and environmental concerns, interest in new energy sources is growing. Solid Oxide Fuel Cell (SOFC) integrated in Micro Gas Turbine (MGT) is a promising and preferred method for generating electric power in the future, having a high efficiency and low pollution.

Transients in the load may have a significant impact on the life of the SOFC/MGT hybrid power system. One of the reasons is that load transients often involve significant peaks in power relative to the steady-state load. Therefore, the primary control goal for the SOFC/MGT hybrid system is to allow the power plant to deliver the desired power output.

There have been very few reports on controlling the power of the SOFC/MGT hybrid system during the last several decades. In Refs. [1,2], a dynamic model was presented for control of the integrated SOFC and turbine hybrid system and the power supplied by the SOFC system was controlled by manipulating the fuel. In Ref. [3], an unstable power output was observed due to the fluctuation of gas composition in the fuel. A specially designed fuel controller succeeded not only in allowing the hybrid system to follow a step change of power demand, but also maintained the system power output stable. However, the SOFC/MGT hybrid system is a multivariable and strong coupling nonlinear system. This coupling affects the effectiveness of a specific loop controller on the corresponding output, and in some case, may become serious and cause many difficulties to the control system design. How the power system is decoupled and practical controllers are designed does not feature currently in the open literature.

In recent years, various linearization and decoupling methods have been presented to handle this problem. The usual methods are based on differential geometry method, which solve a group of differential equations and linearize nonlinear system with state feedback [4–6]. However, the SOFC/MGT hybrid system is an uncertain nonlinear system. It is very difficult to describe such a system with a precise mathematical model.

Neural networks are considered as an attractive structure to establish the mathematical relationship of the dynamic system based on the input–output data. As a kind of recurrent neural network, the OIF Elman neural network is more ascendant than the static neural network such as BP and RBF neural network on the dynamic characteristic. Thereby, it is now widely used in the areas of system identification, nonlinear control and prediction control [7–10]. Furthermore, based on the modified OIF Elman neural network, an adaptive proportional-integral-derivative (PID) decoupling control scheme is proposed to control the SOFC output power and MGT output power. The traditional PID controller is widely applicable in many fields due to

* Corresponding author. Tel.: +86 28 61830661; fax: +86 28 61830662.
E-mail address: xj2_wu@hotmail.com (X.-J. Wu).

0378-7753/$ – see front matter © 2010 Elsevier B.V. All rights reserved.
doi:10.1016/j.jpowsour.2010.07.095

Nomenclature

p_j	gas pressure at state j (atm)
W_j	gas mole flowrate at state j (mol s^{-1})
$W_{j,i}$	mole flowrate of gas i at state j (mol s^{-1})
x_j	molar fraction of gas i
$x_{j,i}$	molar fraction of gas i at state j
τ	moment of inertia (kg m^2)
R	gas constant (8.314 J mol^{-1} K^{-1})
V_{an}	anode volume (cm^3)
V_{ca}	cathode volume (cm^3)
i	SOFC stack current (A)
Q_3	enthalpy of gas i at state j (J mol^{-1})
ε_t	turbine pressure ratio
η_t	turbine efficiency
$h_{j,i}$	gas enthalpy at state j (J mol^{-1})
T_j	gas temperature at state j (K)
N	SOFC number
P_{ac}	stack AC output power (kW)
v_{st}	stack output voltage (V)
P_{st}	stack output power (kW)
P_{MGT}	MGT power (kW)
P_t	turbine power (kW)
η_{ac}	DC/AC conversion efficiency
η_{dc}	DC/DC conversion efficiency
η_m	turbine mechanical efficiency
W_1	air flowrate (mol s^{-1})
W_6	fuel flowrate (mol s^{-1})
n	rotational speed (rpm)
η_r	compressor isentropic efficiency
ε_r	compressor pressure ratio
T_s	SOFC stack temperature (K)
P_{r2}	consumed power by the fuel compressor (kW)

Subscripts

CH_4	methane
CO	carbon monoxide
CO_2	carbon dioxide
N_2	nitrogen
O_2	oxygen
H_2	hydrogen
H_2O	water (gas)
i	state i
j	gas species j

its simplicity and robustness [11–13]. However the SOFC/MGT hybrid system is a complex coupling nonlinear system, which can hardly be solved by the conventional PID controller with fixed parameters. Thus here, the self-learning ability of the OIF Elman neural network is used to tune the PID parameters on-line. The coupling is treated as an exterior disturbance, so the proposed controller is used to eliminate disturbance and improve the tracking performance. A power mathematical model of a 220 kW SOFC/MGT hybrid system is used to generate the data required for the training and prediction of the OIF Elman neural network model.

This paper is outlined as follows: Section 2 briefly describes the SOFC/MGT hybrid power system. In Section 3, a power mathematical model of the hybrid system is built with MATLAB to imitate the real 220 kW SOFC/MGT system. An adaptive PID decoupling control strategy based on the modified OIF Elman neural network is presented for power decoupling control of the SOFC/MGT hybrid system in Section 4. The responses of the SOFC/MGT hybrid system to certain load changes are studied in Section 5. Conclusions and suggestions for future work are finally made in Section 6.

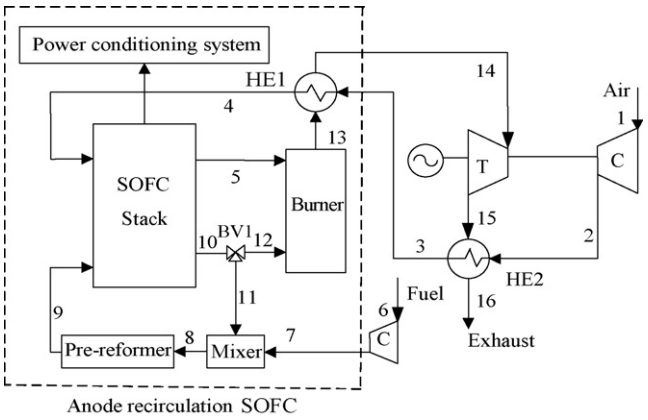

Fig. 1. Structure diagram of SOFC/MGT hybrid power system.

2. Description of SOFC/MGT hybrid power system

The heart of the SOFC/MGT hybrid power system is the internal reforming SOFC (IR-SOFC) stack, which is designed here on the basis of the tubular technology pioneered by Siemens Westinghouse in the 1970s [14]. In order to avoid excessive thermal stresses in the stack, the SOFC operating temperature requires preheating the fuel and air streams. Thus, it is mandatory to use heat exchangers that can transfer the high thermal energy rates of SOFC outlet streams increasing the air and fuel inlet temperature. The steam needed to support the internal reforming reaction is obtained by re-circulating part of the anode outlet stream, which should be controlled to supply sufficient steam to meet the steam and carbon ratio. Therefore, a pressurized SOFC/MGT hybrid power system is designed in this paper, shown in Fig. 1. It consists of an anode recirculation SOFC and a micro gas turbine. The operation process of the SOFC/MGT hybrid system has been described in the Ref. [25].

3. Power mathematical model of SOFC/MGT hybrid power system

Certain assumptions are made in developing the dynamic model for the SOFC/MGT hybrid generation system. These assumptions are all valid from an analytical modeling point of view.

- Gas mixtures are resolved for CH_4, CO, CO_2, H_2, H_2O, N_2, and O_2. All other species are assumed negligible for thermodynamics.
- Both air and fuel are assumed as the ideal gas, which makes them satisfy the ideal gas state equation.
- There is surplus oxygen available for complete combustion due to the fact that air mass flowrate is much larger than the fuel mass flowrate in the burner.
- No heat transfer to the environment. The system is assumed to be well insulated from the environment.
- Each cell in the stack is assumed to operate identically, so that a single SOFC simulation is taken as representative and used to calculate full stack performance.
- Control volumes are characterized by a single lumped temperature, pressure, and species mole fractions condition.

3.1. Valve and mixer model

In order to supply steam for the reforming process, a certain part of the anode exhaust gas must be recycled. The valve is used for the

control of fuel and gas flows. It is adiabatic and fluid inertia is not considered. Flowrate and molar composition of the input and the output are set equal at any load. In the mixer, the amount of steam supplied to the pre-reformer is determined by the steam carbon ratio λ_{sc}, defined as the ratio between the supplied steam to the cell and the supplied methane.

3.2. Pre-reformer model

The supplied fuel is reformed to hydrogen and carbon monoxide by fuel reforming reaction (Eq. (1)) and water-gas shifting reaction (Eq. (2)) in the pre-reformer.

$$CH_4 + H_2O \leftrightarrow CO + 3H_2 \quad (1)$$

$$CO + H_2O \leftrightarrow CO_2 + H_2 \quad (2)$$

Therefore, the energy balance for the pre-reformer is given by:

$$C_{re} \cdot \frac{dT_9}{dt} = \sum_i (W_8 \cdot x_{8,i} \cdot \bar{h}_{8,i}) - \sum_i (W_9 \cdot x_{9,i} \cdot \bar{h}_{9,i}) + Q_r + Q_s \quad (3)$$

where C_{re} is the heat capacity of reformer, Q_r and Q_s the consumed heat by the reforming reaction Eq. (1) and the shifting reaction Eq. (2), which can be calculated as follows:

$$Q_r = r_{re,1} \cdot (\bar{h}_{9,CO} + 3\bar{h}_{9,H_2} - \bar{h}_{8,H_2O} - \bar{h}_{8,CH_4}) \quad (4)$$

$$Q_s = r_{re,2} \cdot (\bar{h}_{9,CO_2} + \bar{h}_{9,H_2} - \bar{h}_{8,H_2O} - \bar{h}_{8,CO}) \quad (5)$$

Under the ideal gas supposition, the partial molar enthalpy $\bar{h}_{j,i}$ is calculated by the formulation:

$$\bar{h}_{j,i} = \bar{h}_{i,0} + \int_{T_{ref}}^{T_j} c_{j,i}(T)\, dT \quad (6)$$

where $j = 1, 2, \cdots, 16$, $i \in \{CH_4, CO, CO_2, H_2, H_2O, O_2, N_2\}$. $\bar{h}_{i,0}$ is the standard enthalpy of gas i, and T_{ref} is the reference temperature (=298 K). The specific heat $c_{j,i}$ of gas i can be obtained from Ref. [15].

3.3. IR-SOFC model

There are three chemical reactions considered in the SOFC stack. These reactions are the methane reformation reaction (Eq. (1)), water-gas shift reaction (Eq. (2)), and electrochemical reaction (Eqs. (7) and (8)).

$$H_2 + O^{2-} \rightarrow H_2O + 2e^- \quad (7)$$

$$\tfrac{1}{2}O_2 + 2e^- \rightarrow O^{2-} \quad (8)$$

Therefore, to calculate the SOFC stack temperature, three heat sources should be determined, namely: (i) heat consumed by the reforming reaction Q_1; (ii) heat consumed by the shifting reaction Q_2; (iii) heat generated due to the electrochemical reaction in the SOFC stack Q_3. Assuming that temperature is uniform in a stack, the energy balance equation for the SOFC can be expressed as:

$$C_s \cdot \frac{dT_s}{dt} = W_4 \cdot \sum_j (x_{4,j} \cdot \bar{h}_{4,j}) + W_9 \cdot \sum_i (x_{9,i} \cdot \bar{h}_{9,i}) - W_5 \cdot \sum_j (x_{5,j} \cdot \bar{h}_{5,j}) - W_{10} \cdot \sum_i (x_{10,i} \cdot \bar{h}_{10,i}) - P_{st} \quad (9)$$

$$+ \sum_k Q_k \quad (9)$$

where $k = 1, 2, 3$, $i \in \{CH_4, CO, CO_2, H_2, H_2O\}$, $j \in \{N_2, O_2\}$, C_s is the stack heat capacity.

The mass balance for the SOFC is described as follows:

$$\frac{p_{10}V_{an}}{RT_s}\frac{dx_{10,i}}{dt} = W_{9,i} - W_{10,i} + \bar{R}_{r,i} + \bar{R}_{an,i} \quad (10)$$

$$\frac{p_5 V_{ca}}{RT_s}\frac{dx_{5,j}}{dt} = W_{4,j} - W_{5,j} + \bar{R}_{ca,j} \quad (11)$$

where

$$\bar{R}_r = [\, -r_1 \quad r_1 - r_2 \quad r_2 \quad 3r_1 + r_2 \quad -r_1 - r_2 \,] \quad (12)$$

$$\bar{R}_{an} = [\, 0 \quad 0 \quad 0 \quad -r_3 \quad r_3 \,] \quad (13)$$

$$\bar{R}_{ca} = [\, 0 \quad -0.5r_3 \,] \quad (14)$$

The reaction rate of hydrogen corresponding to the electrochemical reaction r_3 is directly related to the current i, which is given in Eq. (15):

$$r_3 = \frac{i \cdot N}{2F} \quad (15)$$

Taking into account ohmic, concentration and activation losses, applying Nernst's equation and Ohm's law, the stack output voltage can be obtained according to Refs. [16–18].

The output power of the SOFC stack P_{st} can be obtained by the equation:

$$P_{st} = i \cdot v_{st} \quad (16)$$

The power conditioning unit is the interface between the SOFC output DC voltage and the AC grid, which consists of a DC/DC converter and a DC/AC inverter. Assuming the DC/DC and DC/AC conversion efficiencies are η_{dc} and η_{ac} respectively, the SOFC output power is given by:

$$P_{ac} = P_{st} \cdot \eta_{dc} \cdot \eta_{ac} \quad (17)$$

3.4. Burner model

In the catalytic combustion burner, the residual fuels from the SOFC are burned away which increases the temperature of the gas. The following reactions are being considered during the combustion:

$$2H_2 + O_2 \rightarrow 2H_2O \quad (18)$$

$$2CO + O_2 \rightarrow 2CO_2 \quad (19)$$

The temperature of the product gas can be determined from:

$$C_b \cdot \frac{dT_{13}}{dt} = \sum_i (W_5 \cdot x_{5,i} \cdot \bar{h}_{5,i} + W_{12} \cdot x_{12,i} \cdot \bar{h}_{12,i}) + \sum_j Q_j - \sum_i W_{13} \cdot x_{13,i} \cdot \bar{h}_{13,i} \quad (20)$$

where, $i \in \{CO, CO_2, H_2, H_2O, O_2, N_2\}$, $j \in \{H_2, CO\}$, Q_j is the combustion heat of H_2 and CO respectively.

3.5. Heat exchanger model

Compact heat exchangers are often used in recuperated gas turbine cycles. As one kind of compact heat exchanger, plate-fin heat exchanger is chosen in this model. The dynamics of the heat exchanger are described in Ref. [19].

3.6. Compressor model

The compressor map is based on a DLR centrifugal compressor map, while the turbine map is for a NASA-CR-174646 axial turbine [20]. The original and smoothened data files of these turbomachines are obtained from the manufacturers. According to the similarity

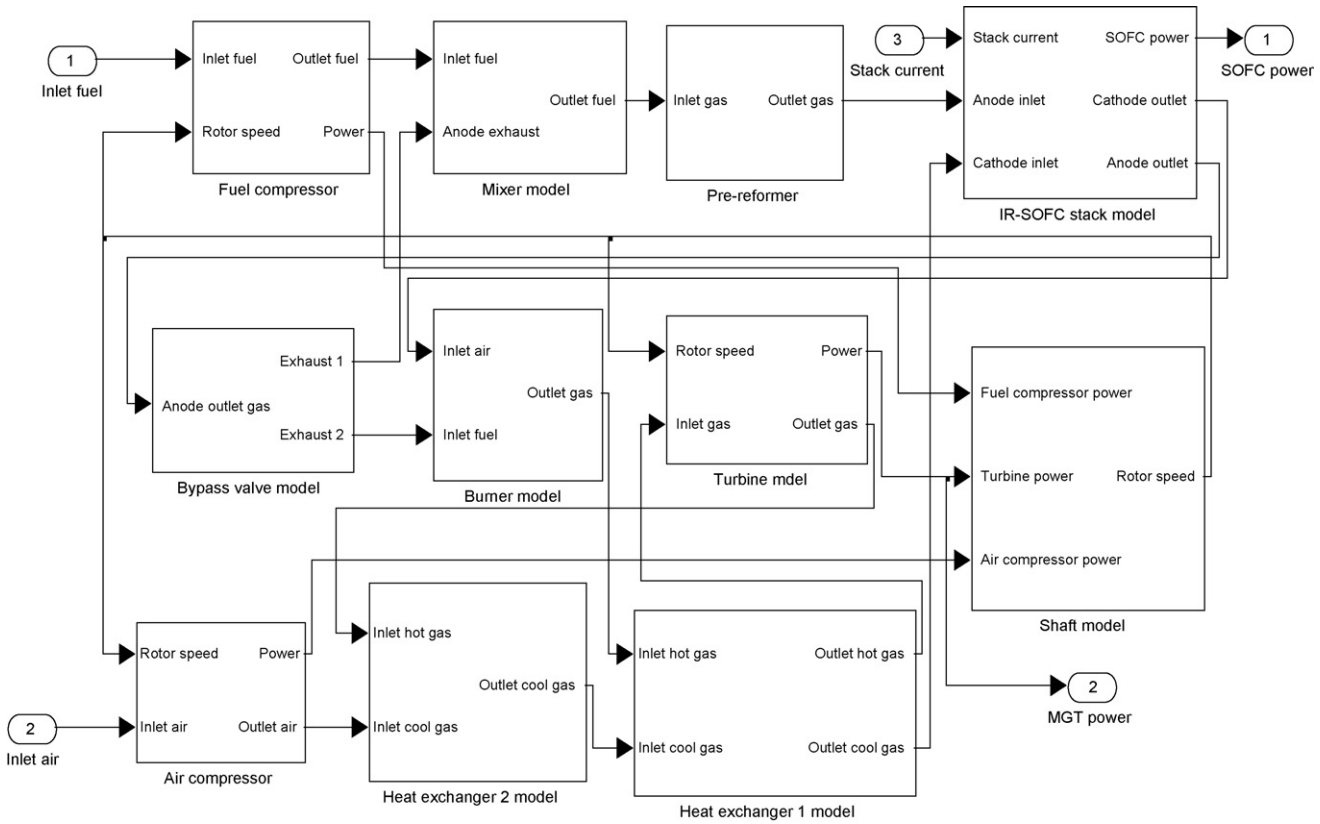

Fig. 2. SOFC/MGT hybrid power system model in SIMULINK.

theory, the features of the compressor can be described as a function of the pressure ratio, reduced mass flow, reduced speed and efficiency.

When the operational point is located, pressure ratio, isentropic efficiency and flowrate are known, the exit temperature T_2 of the air compressor can be expressed as follows:

$$T_2 = T_1 + \frac{T_1}{\eta_r} \cdot (\varepsilon_r^{(r_1-1)/r_1} - 1) \tag{21}$$

where adiabatic coefficient r_1 can be obtained from Ref. [21].

The consumed thermal power by the air compressor, P_{r1}, can be calculated from the following equation:

$$P_{r1} = W_1 \cdot (\bar{h}_2 - \bar{h}_1) \tag{22}$$

3.7. Turbine model

The compressor and gas turbine are assumed to be coupled on a single shaft. As a consequence, they have the same rotor speed. The maps are used to calculate the pressure ratio and isentropic efficiency as a function of mass flowrate and rotor speed .The ideal temperature of the working fluid at the outlet of the turbine can be evaluated using Eq. (23).

$$T_{15} = T_{14} - T_{14}\,(1 - \varepsilon_t^{1-n_{14}/n_{14}})\,\eta_t \tag{23}$$

The turbine work can be calculated from the real enthalpy change and the flowrate, which is expressed as follows:

$$P_t = W_{14} \cdot (\bar{h}_{14} - \bar{h}_{15}) \tag{24}$$

3.8. Shaft model

A shaft model accounts for the dynamics of the rotating mass in the gas turbine system, which is modeled as follows:

$$\frac{dn}{dt} = \frac{900}{n\tau\pi^2} \cdot P_{MGT} \tag{25}$$

where τ is the moment of inertia. Neglecting the generator mechanical loss, the output mechanical power from the gas turbine P_{MGT} is defined in the following equation:

$$P_{MGT} = \eta_m \cdot P_t - P_{r1} - P_{r2} \tag{26}$$

The power mathematical model replaces the real SOFC/MGT hybrid power system to generate the simulation data required for the identification of the modified OIF Elman neural network model. For the SOFC/MGT dynamic physical model, the SOFC output power and MGT output power are the controlled variables, fuel flowrate and air flowrate are chosen as manipulated variables, and the load current is considered as a disturbance. The SOFC/MGT hybrid power system model developed in MATLAB is shown in Fig. 2. The parameters of the SOFC/MGT hybrid system are given in Table 1.

4. Power decoupling control of SOFC/MGT hybrid power system

4.1. Power control strategy

The structure for the power decoupling control of the SOFC/MGT hybrid system is shown in Fig. 3, which combines the modified OIF Elman neural network and the PID controller.

In Fig. 3, $m = 1, 2$, $r_m(k)$ is the reference power (SOFC output power and MGT output power), $y_m(k)$ the real output power, $ym_m(k)$ the modified OIF Elman neural network identification

Table 1
Setting parameters used in the model of SOFC/MGT hybrid system.

Parameter	Unit	Value
Cell number N	–	1152
Active area A	cm^2	834
DC/DC conversion efficiency η_{dc}	–	97%
DC/AC conversion efficiency η_{ac}	–	97%
Compressor pressure ratio ε_r	–	2.9
Compressor isentropic efficiency η_r	–	78%
Turbine isentropic efficiency η_t	–	82%
Steam/Carbon ratio λ_{sc}	–	2.5
Turbine mechanical efficiency η_m	–	94%
Moment of inertia τ	$kg\,m^2$	0.00127
Stack heat capacity C_s	$J\,K^{-1}$	471

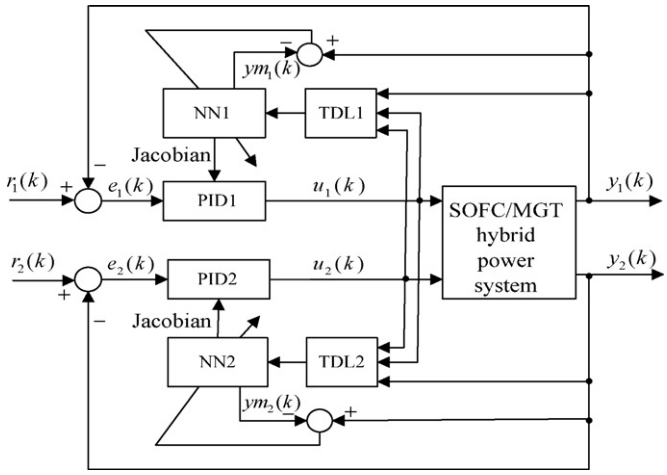

Fig. 3. Power decoupling controller structure of the SOFC/MGT system.

power, $e_m(k)$ the error between the given value $r_m(k)$ and output $y_m(k)$ in every instant, $u_m(k)$ the manipulated variable. According to the error $e_m(k)$, the modified OIF Elman neural network identification model is used to tune the parameters of the conventional PID controller to keep the system stable. For two inputs and two outputs system, the coupling effect from the second loop is treated as exterior disturbance to the first main loop. At the same time, the coupling effect from the first loop is treated as exterior disturbance to the second main loop. Thereby, the PID controller based on the modified OIF Elman neural network is used to eliminate disturbance and improve the tracking performance.

4.2. Modified OIF Elman neural network model

The following NARX model is used to describe the controlled power system:

$$y(k) = f[y(k-1), \ldots, y(k-n_y), u(k-1), \ldots, u(k-n_u)] \quad (27)$$

where y is the SOFC output power and MGT output power, u is the fuel flowrate, air flowrate and current, n_y and n_u are the lags of the output and input respectively, and $f(\cdot)$ is a nonlinear function. In this section, we adopt a modified OIF Elman neural network identification model to identify the nonlinear function $f(\cdot)$.

The OIF Elman neural network is a type of recurrent neural network, which has two particular layers called the context layer and the context 2 layer besides the conventional input, hidden and output layers. The context layer and context 2 layers are used to memorize the former values of the hidden and output layer nodes respectively. The feed-forward connections are modifiable, whereas the recurrent connections are fixed. The structure of OIF Elman neural network is shown in Fig. 4 [22].

In Fig. 4, w^u is the weight between the input layer and hidden layer, w^y is the weight between the hidden layer and the output

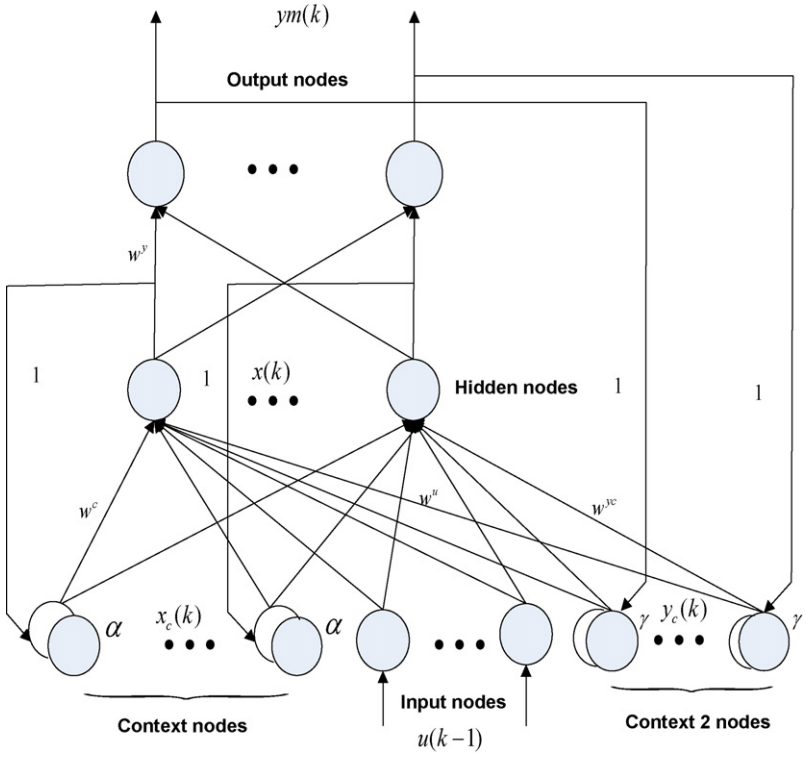

Fig. 4. Structure of OIF Elman neural network.

layer, w^c is the weight from the context layer to the hidden layer, and w^{yc} is the weight from the context 2 layer to the hidden layer. $x_c(k)$ and $x(k)$ are the outputs of the context unit and the hidden unit respectively. $y_c(k)$ and $ym(k)$ are the outputs of the context 2 layer and output layer respectively. α and γ are the feedback gains of the self-connections of context and context 2 layers respectively, $0 \le \alpha < 1$, $0 \le \gamma < 1$.

The mathematical model of the OIF Elman neural network is described as follows:

$$x(k) = f(w^c x_c(k) + w^u u(k-1) + w^{yc} y_c(k)) \tag{28}$$

$$x_c(k) = \alpha \cdot x_c(k-1) + x(k-1) \tag{29}$$

$$y_c(k) = \gamma \cdot y_c(k-1) + y(k-1) \tag{30}$$

$$ym(k) = g(w^y x(k)) \tag{31}$$

where $g(x)$ is often taken as a linear function, and $f(x)$ is often taken as a sigmoid function, namely:

$$f(x) = \frac{1}{1+e^{-x}} \tag{32}$$

The standard Elman network usually adopts BP algorithm to train the network's weights, however it is easy to get locked into local minima [23]. Therefore, here an improved particle swarm optimization is adopted to train the weights of the OIF Elman neural network [24]. The main steps can refer to the optimization process of Ref. [25].

4.3. Self-tuning PID decoupling control based on modified OIF Elman model

The digital incremental PID control algorithm is adopted here, which is expressed as follows:

$$u_m(k) = u_m(k-1) + k_{pm}x_m(1) + k_{im}x_m(2) + k_{dm}x_m(3) \tag{33}$$

where

$$x_m(1) = e_m(k) - e_m(k-1) \tag{34}$$

$$x_m(2) = e_m(k) \tag{35}$$

$$x_m(3) = e_m(k) - 2e_m(k-1) + e_m(k-2) \tag{36}$$

where k_{pm}, k_{im} and k_{dm} are the proportional factor, integral factor and differential factor respectively.

Define the performance index H_m as follows:

$$H_m(k) = \frac{1}{2}[e_m(k)]^2 = \frac{1}{2}[r_m(k) - y_m(k)]^2 \tag{37}$$

Adopting the gradient descent method, k_{pm}, k_{im} and k_{dm} are adjusted as per the following:

$$k_{pm}(k) = k_{pm}(k-1) - \eta_p \frac{\partial H_m}{\partial k_{pm}} = k_{pm}(k-1) + \eta_p e_m(k) \frac{\partial y_m}{\partial u_m} x_m(1) \tag{38}$$

$$k_{im}(k) = k_{im}(k-1) - \eta_i \frac{\partial H_m}{\partial k_{im}} = k_{im}(k-1) + \eta_i e_m(k) \frac{\partial y_m}{\partial u_m} x_m(2) \tag{39}$$

$$k_{dm}(k) = k_{dm}(k-1) - \eta_d \frac{\partial H_m}{\partial k_{dm}} = k_{dm}(k-1) + \eta_d e_m(k) \frac{\partial y_m}{\partial u_m} x_m(3) \tag{40}$$

where η_p, η_i and η_d are the proportion, integral and differential learning rate respectively, $\partial y_m / \partial u_m$ is the Jacobian information of controlled object, which can be obtained from the above modified OIF Elman identification results, i.e. $\partial y_m / \partial u_m \approx \partial ym_m / \partial u_m$.

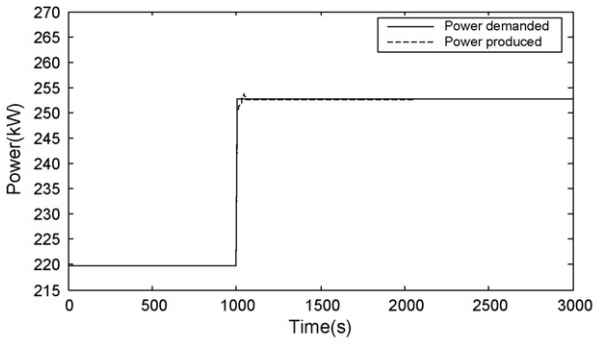

(a) Response of the SOFC/MGT output power

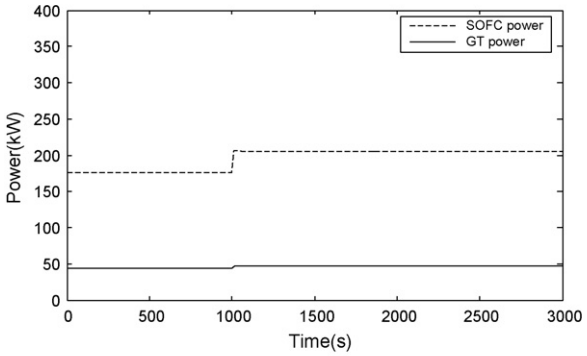

(b) Response of the SOFC output power and MGT output power

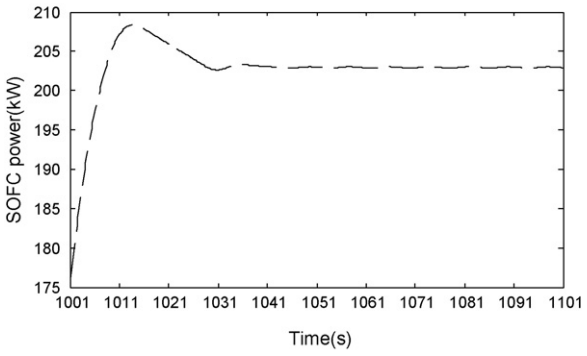

(c) Response of the SOFC output power in [1001s,1101s]

Fig. 5. Response of the SOFC/MGT output power during +15% step change.

5. Simulation

In this section, we present numerical experiments to validate the proposed adaptive PID decoupling control scheme based on the modified OIF Elman identification model of the SOFC/MGT hybrid system.

From the above mentioned Sections 2 and 3, firstly, based on the mass balance and enthalpy balance equations, the power mathematical model of the SOFC/MGT hybrid system described in Section 2 is built with MATLAB to imitate the real 220 kW SOFC/MGT hybrid system in Section 3. With the mathematical model, the training data for the modified OIF Elman neural network model is generated. In order to obtain available identification data, the input signals of the power physical model are uniformly random, including the fuel flowrate, air flowrate and the current. A set of 600 data is collected from the simulation. The first 400 data are used for the identification of the modified OIF Elman neural network identification model, while the remaining 200 data are used for validation purposes.

In this study, Kolmogorov theorem is used to determine the number of hidden node, and is given as $2r+1$, where r is num-

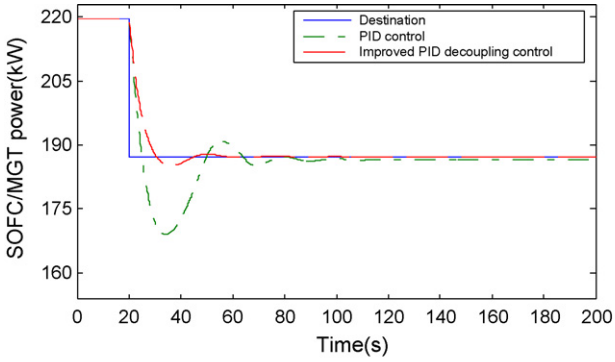

(a) Response of the SOFC/MGT output power

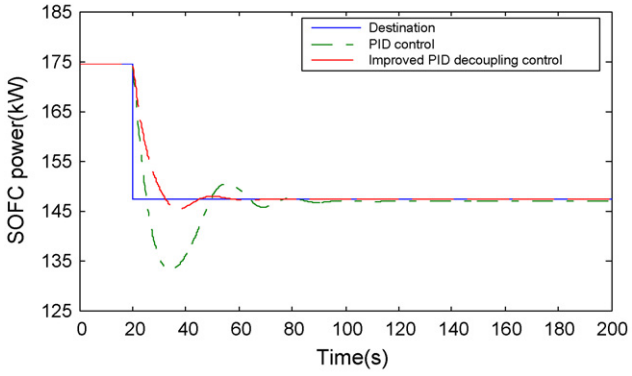

(b) Response of the SOFC output power

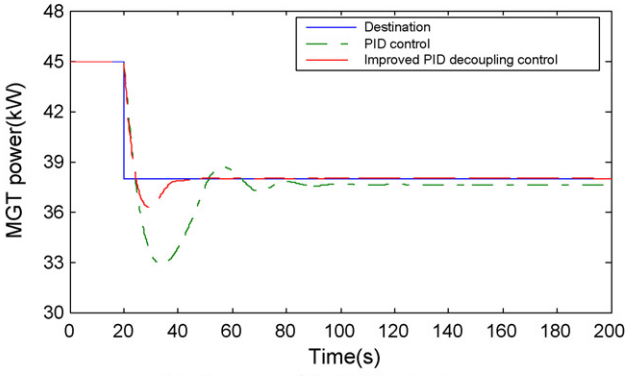

(c) Response of the MGT output power

Fig. 6. Response of the SOFC/MGT output power during −15% step change.

ber of input units. There are three inputs (air flowrate W_1, fuel flowrate W_6 and current i). So, the hidden layer of the modified OIF Elman neural network is calculated to be 7 nodes. Here, the improved PSO algorithm is applied to obtain the weights of the OIF Elman neural network. Therefore, each particle consists of $3\times7+7\times2+7\times7+2\times7$ parameters, and all weights are chosen on the interval [−1, 1]. The parameters of the improved PSO algorithm are set as follows: swarm size m is 40, maximum number of iterations $G_{\max}$ is 200, accelerating factors c_1 and c_2 are 1.8, maximum inertia weight $\varpi_{\max}$ is 0.9, minimum inertia weight $\varpi_{\min}$ is 0.1, step size of the inertia weight $\Delta\varpi$ is 0.05. Using MATLAB to run the program of the modified OIF Elman model and after 200 iterations, the optimal weights of OIF Elman can be determined.

Based on the modified OIF Elman neural network model, the adaptive PID decoupling controller is used to control the power of the SOFC/MGT hybrid system. Firstly assume that the external load of the SOFC/MGT hybrid system has a +15% step change at 1000 s. The simulation time is 3000 s, and the sampling time is 0.1 s. The proportion, integral and differential learning rate are $\eta_p = 0.09$, $\eta_i = 0.3$ and $\eta_d = 0.2$ respectively. The PID parameters k_p, k_i and k_d are adjusted by self-learning modified OIF Elman neural network until the error approach zero. The simulation results are shown in Fig. 5. The output power of the SOFC/MGT hybrid system tracts and decouples the reference power satisfactorily, which is shown in Fig. 5(a). The maximum error of the output power is 1.02%, and the mean steady-state error is 0.03%. The response of the SOFC output power and the MGT output power are shown in Fig. 5(b). The specific change of the SOFC from 1001 s to 1101 s is shown in Fig. 5(c). In order to compare with the traditional PID control, now assuming the external load of the SOFC/MGT hybrid system has a −15% step change at 20 s, the simulation results are shown in Fig. 6. From Fig. 6, the traditional PID controller is incapable of controlling the output power to the target value. However, using the improved PID decoupling control method, the SOFC/MGT output power can effectively tract the reference power. The maximum error of the output power is 1.58%, and the mean steady-state error is 0.06%. In addition, as the SOFC output power is the core output power of the hybrid system, the variation curve of the SOFC/MGT output power is similar to the SOFC output power.

6. Conclusions

In order to allow the SOFC/MGT hybrid power system to deliver the desired power output, this paper employs an adaptive PID decoupling controller based on a modified OIF Elman neural network identification model to control the SOFC output power and MGT output power. The data required for the training and prediction of the modified OIF Elman neural network identification model is generated from a power mathematical model of a 220 kW SOFC/MGT hybrid power system. The simulation results show that the proposed adaptive PID decoupling control algorithm based on the modified OIF Elman neural network model is an efficient method to solve the nonlinear coupling power system for the SOFC/MGT hybrid system. In order to develop an integrated control strategy, in the future other transient impacts besides current will be further discussed (e.g., ambient temperature, pressure fluctuations and fuel composition changes).

Acknowledgment

This work is supported by National Natural Science Foundation of China (no. 50977007)

References

[1] C. Stiller, B. Thorud, O. Bolland, Journal of Power Sources 158 (2006) 303–315.
[2] R. Roberts, J. Brouwer, F. Jabbari, et al., Journal of Power Sources 161 (1) (2006) 484–491.
[3] T. Kaneko, J. Brouwer, G.S. Samuelsen, Journal of Power Sources 160 (1) (2006) 316–325.
[4] D.N. Godbole, S.S. Sastry, IEEE Transactions on Automatic Control 40 (3) (1995) 441–450.
[5] Y. Zhang, J. Wang, Automatica 37 (2001) 1161–1173.
[6] Y. Zhang, J. Wang, IEEE Transactions on Neural Networks 13 (3) (2002) 633–644.
[7] M.F.A. Aziz, H.N.A. Hamed, S.M.H. Shamsuddin, Proceedings of the 2008 Second Asia International Conference on Modelling & Simulation, Piscataway, NJ, USA, 2008, pp. 625–630.
[8] Q.H. Cao, S.A. Wang, Computer Engineering and Application 43 (31) (2007) 87–89.
[9] X. Hui, Y.H. Sun, C.Y. Sun, Xia, Transactions of CSICE 25 (4) (2007) 352–357.
[10] W.M. Qi, Y.C. Cheng, Q.L. Ji, et al., Control and Decision 20 (10) (2005) 1197–1200.
[11] R. Kumar, R.A. Gupta, B. Singh, IEEE International Conference on Information Technology, Piscataway, NJ, USA, 2007, pp. 2055–2060.
[12] C.G. Xu, D.M. Lue, J. Hao, Journal of Beijing Institute of Technology 17 (3) (2008) 270–273.
[13] S. Gang, S.X. Yang, Y.X. Jing, et al., Journal of Beijing Institute of Technology 17 (1) (2008) 58–61.

[14] J. Larminie, A. Dicks, Fuel Cell Systems Explained, Wiley, New York, 2004.
[15] B. Liu, R. Lu, Physical and Chemistry, Huazhong University of Science and Technology, 2008.
[16] S. Campanari, P. Iora, Journal of Power Sources 132 (1-2) (2004) 113–126.
[17] R. Bove, P. Lunghi, N.M. Sammes, International Journal of Hydrogen Energy 30 (2) (2005) 181–187.
[18] X.J. Wu, X.J. Zhu, G.Y. Cao, et al., Simulation Modeling Practice and Theory 16 (5) (2008) 494–504.
[19] Q.M. Chen, PhD Thesis, Shanghai Jiao Tong University, 2007.
[20] J. Kurzke, Compressor and Turbine Maps for Gas Turbine Performance Computer Programs-Component Map Collection, vol. 2, Joachim Kurzke, Dachau, Germany, 2004.
[21] D.C. Zeng, Engineering Thermodynamics, third edition, Higher Education Press, Beijing, 2002.
[22] X.H. Shi, Y.C. Liang, H.P. Lee, et al., Applied Artificial Intelligence 18 (2004) 603–629.
[23] G. Yang, X.C. Yuan, IEEE International Conference on Wireless Communications, Networking, and Mobile Computing, Piscataway, NJ, USA, 2007, pp. 5667–5670.
[24] N. Iwasaki, K. Yasuda, G. Ueno, Transaction on Electrical and Electronic Engineering 1 (4) (2006) 353–363.
[25] X.J. Wu, Q. Huang, X.J. Zhu, International Journal of Hydrogen Energy. Accepted.